JOURNAL OF CATALYSIS 104, 109–119 (1987)

A Surface Science Investigation of the Water-Gas Shift Reaction on Cu(111)

CHARLES T. CAMPBELL* AND K. A. DAUBE†

*Chemistry Department, Indiana University, Bloomington, Indiana 47405 and †Chemistry Division, Los Alamos National Laboratory, Los Alamos, New Mexico 87545

Received July 30, 1986; revised October 7, 1986

We have studied the kinetics of the water-gas shift reaction on a clean Cu(111) single-crystal surface using an apparatus which allows rapid transfer of the catalyst between a microreactor and an ultrahigh-vacuum chamber for surface preparation and postreaction surface analyses (AES, XPS, LEED). At 10 Torr H_2O, 26 Torr CO, and 612 K, the reaction proceeds with an activation energy of 17 kcal mole^{-1} and reaction orders in H_2O and CO pressures of zero and 0.5–1.0, respectively. The surface appears completely metallic and relatively free of adsorbed species in postreaction analysis, even when heavily preoxidized. The kinetics compare favorably with data for high-surface-area Cu/ZnO or Cu-based catalysts, indicating that metallic Cu is the active ingredient in these. The rate is limited by dissociative adsorption of water under our conditions. We were unable to produce significant coverages of oxygen species on Cu(111) by dosing pure H_2O at 10 Torr and 500–650 K. The mechanism is discussed in light of surface science measurements on Cu surfaces. The Cu(111) surface was also dosed with Zn from aqueous solution, and the resulting ZnO_x/Cu(111) surfaces were tested for activity as water-gas shift catalysts. No marked changes in activity compared to clean Cu(111) were observed. A new method for increasing gas chromatographic sensitivities for low sampling pressures (<1 atm) is also described.

I. INTRODUCTION

The solid-catalyzed, forward water-gas shift reaction ($H_2O + CO \rightarrow CO_2 + H_2$) is a step in numerous industrial processes, including hydrogen production (for its own sake and in combustion cleanup) and ammonia synthesis. To efficiently utilize our fossil fuel resources, a number of large-scale industrial processes demanding hydrogen are expected to appear in the future. Coal gasification, for example, may rely on water-gas shift catalysts to upgrade the hydrogen content for down stream reactions such as methanation or methanol synthesis. In spite of its importance, not much has been published concerning this reaction (see *(1–11)* and ref. therein). Many materials catalyze water-gas shift (WGS) *(1–11)*. The traditional iron-based catalysts have been replaced in many industrial applications with copper-based catalysts, which operate at lower temperatures, allowing higher thermodynamic conversions. These usually contain ZnO as a "promoter or structural stabilizer," although the exact role of ZnO is not yet clear *(1–8)*. A disadvantage of Cu-based catalysts, particularly with respect to coal- or petroleum-derived feedstreams, is that they are highly susceptible to sulfur poisoning *(1)*.

In order to understand the relationship between surface structure and the activity of WGS catalysts, we have undertaken a program to investigate the catalytic properties of a series of model, Cu-based catalysts which are extremely homogeneous and well-characterized with respect to their surface structure. The present work describes medium-pressure kinetics of the WGS reaction over a clean Cu(111) single-crystal surface, as well as pre- and postreaction surface analyses under ultrahigh vacuum (UHV). To our knowledge, these are the first measurements of the water-gas shift reaction over any single-crystal catalyst. Ki-

0021-9517/87 $3.00

netics on a Zn-doped Cu(111) surface have also been tested here. Results on sulfur poisoning (*12*) and cesium promotion (*13*) of this Cu(111) model catalyst will be presented elsewhere.

II. EXPERIMENTAL

These experiments were performed in an apparatus, described in detail elsewhere (*14*), which combines an UHV chamber for surface analyses (XPS, AES, LEED, TDS) with a microreactor for high-pressure ($\leq$10 atm) catalytic kinetics on small-area (~1 cm^2) samples. The Cu(111) crystal was mounted on a rod for rapid (~17 s) transfer between the stages.

The crystal was cut and oriented as usual, mechanically polished to a mirror finish, then chemically polished with a warm solution of 66% glacial acetic acid, 17% phosphoric acid, and 17% nitric acid (while rubbing with cotton). It was mounted on the transfer rod as in (*14*) for resistive heating and temperature control. The front sample surface was routinely Ar^+ sputter cleaned at 770 K, followed by a brief (30–120 s) anneal at ~890 K. This gave an extremely bright and sharp $p(1 \times 1)$ LEED pattern, and no other species except Cu by AES, XPS, and ISS (1 KeV He^+). The crystal dimensions were $10 \times 7 \times 1.3$ mm. Coverages (θ) are quoted with respect to the Cu(111) atom density (1.76×10^{15} cm^{-2} or $\theta = 1$).

The sample was cleaned and characterized under UHV (~1×10^{-10} Torr), then translated to the evacuated microreactor, which was then pressurized with the reactant mixture. The sample was then rapidly heated to the reaction temperature and maintained at that temperature for the desired reaction time. Since the walls of the microreactor were at room temperature, we were limited to the vapor pressure of water as its maximum reactant pressure (<18 Torr). After reaction, the sample (at reaction temperature) was rapidly (~17 s) translated to the UHV chamber, where the pressure rose to ~10^{-7} Torr due to water outgassing from the sample region. The sample was then allowed to cool. The pressure dropped in <2 min to 10^{-8} Torr or better, depending on the H_2O pressure used for the reaction. Liquid nitrogen cryopanels were often used here to help pump. When the pressure was below 5×10^{-9} Torr, surface analysis was initiated. In cases where postreaction surface analysis was not critical, the sample was stopped at an intermediate turbo-pumped stage for 2 min for pumping, to minimize water load in the UHV chamber.

The product buildup in the batch microreactor (volume = 32 ml) was monitored with thermal conductivity detection gas chromatography (GC). A $\frac{1}{8}$-in. $\times$ 3 ft column (100/120 Carbosieve S-II - Supelco) at 140°C gave efficient separation in <2 min. Use of N_2 as a carrier gas (17 ml min^{-1}) allowed for simultaneous detection of H_2 and CO_2 with very good and nearly equal sensitivities. This was *much* preferable to He carrier. The detector temperature was 250°C.

We found a very useful way of greatly increasing GC sensitivity, by rapidly compressing our low-pressure (~20 Torr) gas aliquot into the GC sampling loop, using high-pressure N_2 gas (~800 Torr) as a sort of piston. This should be of use to anyone studying gas compositions where the sample pressure is between ~1 and 800 Torr. Imagine a very long, thin tube as a sample loop on a standard six-way sampling valve. If this loop is filled with a low-pressure, unknown gas mixture and then switched into the high-pressure carrier flow, the carrier gas will momentarily expand in both directions down this sample loop. This expansion compresses the unknown gas mixture toward the midpoint of the loop, and results in a much more spatially localized sample slug than would be expected from the loop volume. The net result is that one can choose a loop length (and therefore sample volume) that is bigger (than expected from resolution requirements) by a factor equal to the carrier:sample pressure ratio. In our

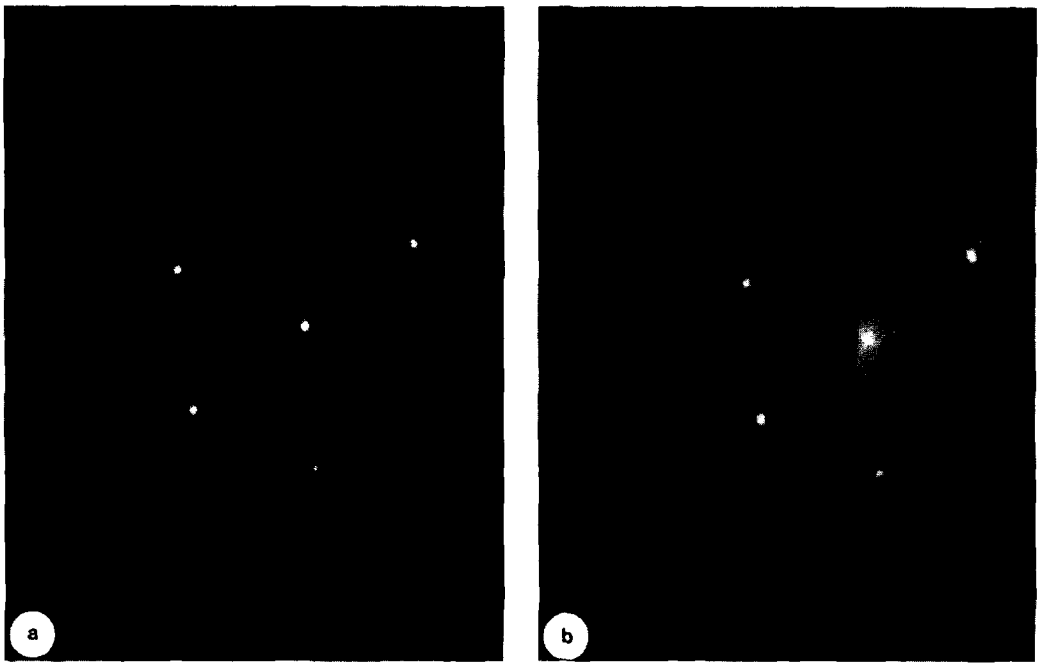

FIG. 1. LEED patterns of Cu(111) at room temperature for near-normal incident beam at 98 eV. (a) clean; (b) with saturated oxygen adlayer (4×10^{-4} Torr s O_2 at 500 K).

case, spatial requirements forced the GC sample loop to be some distance from the reactor, and the total sample available was small. We therefore used a second source of high-pressure N_2 gas to compress the sample along the thin tubing connecting the reactor to the sampling valve and to the sample loop. We then quickly switched this loop into the carrier stream, before the analyte could escape the loop by diffusion. Signal strength was easily increased by a factor of 20 in this way. Two consecutive analyses of the same gas mixture by this method differed on the average by less than 4%.

Reagent grade CO (99.99%) and HPLC grade H_2O (>99.9995) were used here. The H_2O was further purified by numerous freeze–pump–thaw cycles.

III. RESULTS

A. Oxygen Adsorption on Cu(111)

Since we were interested in the oxidation state of the Cu and its surface under reaction conditions, we first reproduced a few results concerning the interaction of O_2 with Cu(111). We found very similar behavior to that reported by Russell *et al.* (*15*), with the surface saturating under vacuum O_2 dosing (4×10^{-4} Torr · s) with an O (510 eV)/Cu (920 eV) peak-to-peak ratio in AES of 0.14 at 500 K. This has been assigned to atomically adsorbed oxygen (O_a) at a coverage $\theta_0 = 0.45$ (*15*). We observed a very complex but distinct LEED pattern for this surface, shown in Fig. 1. To our knowledge this has not been previously observed, although other patterns are seen at higher exposures or temperatures (*16–18*), or below room temperature (*19*). Evidence for O-induced rearrangement of the Cu(111) surface atoms has been presented (*20, 21*). Due to its complexity, we will not speculate here on the structure giving rise to this LEED pattern. In any case, the unit cell is very large. Thus, a very perfect surface would be required for this structure to order itself. This may help explain why only increased

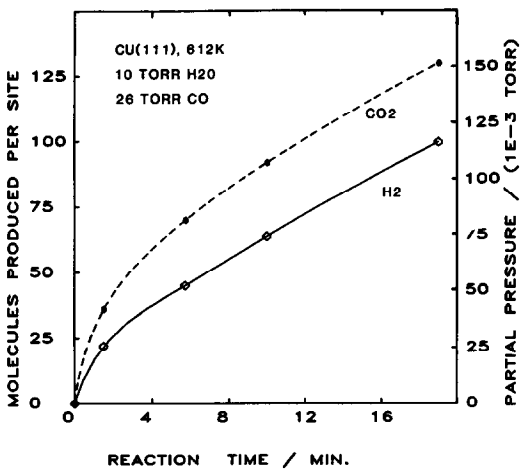

FIG. 2. Buildup of H_2 and CO_2 partial pressures in the batch microreactor (measured by GC) with reaction time for 10 Torr H_2O and 26 Torr CO over Cu(111) at 612 K.

background has been previously observed for such exposures on Cu(111) (*16–23*), although our exact temperature conditions have not been extensively studied.

B. Water-Gas Shift Kinetics on Cu(111)

Figure 2 shows the buildup of H_2 and CO_2 partial pressures in the microreactor (measured by GC) versus reaction time for clean Cu(111) at 612 K, 10 Torr H_2O, and 26 Torr CO. Each data point was necessarily a separate experiment, starting from clean Cu(111) with a fresh gas mixture, since GC sampling reduces the reactor pressure significantly. (Here the surface was sputtered and annealed between runs.) Also shown is a scale for the total number of H_2 and CO_2 molecules produced per surface Cu atom (site), assuming only the front Cu(111) surface contributes to the rate. This is a safe assumption, since only that face was sputter cleaned. The assumption was also confirmed by sulfur poisoning experiments where sulfur was beam dosed *only* onto the *front* Cu surface, yet the rates decreased linearly to zero at saturation coverage (*12*). The back and edges of the crystal were always poisoned, undoubtedly by surface impurities.

One can see in Fig. 2 that the rate (slope) decreases with time, rapidly at first, and then very slowly. The reason for the short-time rate decay is not understood. It could not be associated with any significant change in surface condition as revealed by postreaction surface analysis. Some of this may be associated with outgassing or reactions on the sample holder as it heats. The rate after ~2 min time is almost constant and the same for H_2 and CO_2 production, consistent with the WGS balance: $H_2O + CO \rightarrow H_2 + CO_2$. In the results below, we take the slope between 2 and 12 min reaction time as a quasi-steady-state rate, within the limit of low conversion ($\leq$1%). During that time, about 40 molecules of reactant are converted to H_2 or CO_2 per Cu surface atom.

Surface analysis by AES after reaction revealed low levels of carbon and sulfur impurity. For the data reported here, the tiny sulfur levels ($\theta_s < 0.02$) were too small to significantly affect the ratio (*12*). The carbon level is harder to calibrate, but can be estimated from the signals we obtain for known levels of sulfur (*12*) and oxygen (see above). We then used the AES sensitivity ratios of another analyzer (*24*) for C, O, and S, correcting for a linear ratio of analyzer transmission functions versus energy. In this way we obtain $\theta_c < 0.1$. For cases when the final carbon level differed by a factor of 3 in this region, no significant difference was observed in the reaction rates for otherwise identical reaction conditions. This indicates that the carbon level was at least acceptable here. The irreproducibility of this carbon level indicates that it was not some adsorbed intermediate characteristic of the reaction, but instead due to impurities in the reactor gas. Similar carbon levels appeared when just dosing pure H_2O at ~10 Torr, suggesting that the impurities were displaced from the reactor walls by water adsorption. When the carbon level was at its lowest values, a tiny oxygen signal was also observable in AES after reaction. These signals were too small to analyze for

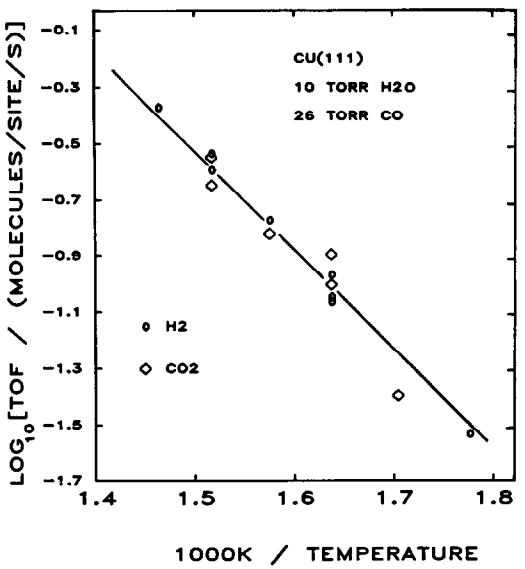

FIG. 3. Site-specific WGS rate versus temperature, in Arrhenius form, for quasi-steady-state conditions in the low-conversion limit over clean Cu(111).

information about the nature of any possible O- or C+O-containing species stable after reaction. A beautiful, sharp $p(1 \times 1)$ LEED pattern of very low background was always observed after reaction. To the extent that our sample transfer into the UHV does not alter the surface structure, these results indicate that the WGS reaction can proceed on an essentially oxygen-free Cu(111) surface.

Figure 3 shows the effect of temperature on the reaction rates, in Arrhenius form, for 10 Torr H_2O and 26 Torr CO. Rates are expressed as a turnover frequency (TOF), i.e., the number of molecules produced per Cu surface atom (site) per second. The data are well fitted by a straight line whose slope indicates an apparent activation energy of 17 kcal mole^{-1} for the WGS reaction on Cu(111).

Figure 4 shows the influence of CO and H_2O partial pressures on the reaction rate at 612 K and constant H_2O or CO pressures of 10 and 26 Torr, respectively. As can be seen, the rate is nearly independent of P_{CO} (order $\simeq$ 0) and strongly positive order in H_2O (0.5–1.0). (The solid curve in Fig. 4 is a fit to the H_2O pressure dependence assuming a reaction order of 0.75.)

To further prove that the Cu surface is fully reduced under WGS conditions at low conversion, we first oxidized the clean Cu(111) surface in 10 Torr O_2 gas at 500 K for 10 min. This surface gave huge oxygen AES and XPS signals, and a Cu(2p) XPS spectrum which was characteristic of bulk CuO (*25*). We then performed the WGS reaction on this surface at 612 K in 10 Torr H_2O, 25 Torr CO. After a few minutes reaction time, the surface displayed a fully metallic Cu(2p) XPS spectrum, and gave no oxygen signal in AES or XPS. The surface is therefore easily reduced to the metallic state under reaction conditions, undoubtedly due to the facile reaction of CO to remove oxygen from Cu surfaces via CO_2 production (*22*).

C. Water Adsorption on Cu(111)

We attempted to oxidize the clean Cu(111) surface or to deposit surface oxy-

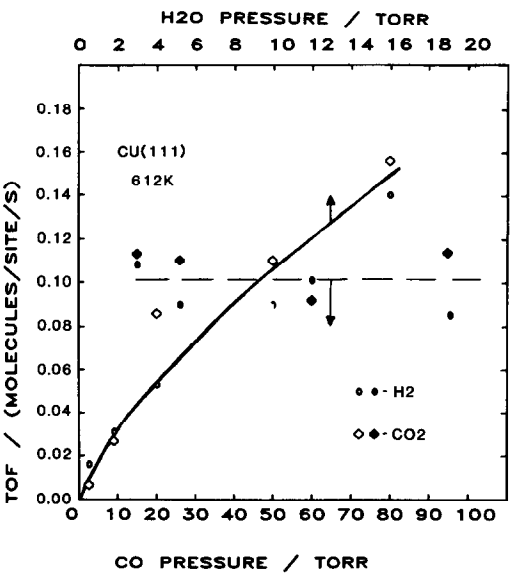

FIG. 4. Effect of reactant partial pressures upon the WGS reaction rate over clean Cu(111) at 612 K. Filled symbols: vary P_{CO}, P_{H_2O} = 10 Torr; open symbols: vary P_{H_2O}, P_{CO} = 26 Torr.

gen by dosing pure H_2O gas in the microreactor at pressures up to 15 Torr and temperatures of 500–650 K. In most cases a tiny, impurity-related carbon AES signal was seen after the high-pressure H_2O dose (see above). In the best cases, this carbon level was almost immeasurable, and a tiny oxygen AES signal was seen. We proved that any atomically adsorbed oxygen, if produced, was not being lost by reactions with background gases during sample transfer from the microreactor by first predosing the surface with a saturation layer of O_a under UHV, then transferring the sample to and from the microreactor at 600 K. No significant loss of O_a was observed. Furthermore, any impurities in the microreactor with the H_2O which could remove O_a by reactions should eventually be consumed by these very reactions; and, O_a should finally predominate, if it were produced on the surface. The concentration of such reactive impurities is certainly $\ll 1\%$, which sets a conservative upper limit of 10^{-6} on the reaction probability of H_2O to yield O_a on Cu(111) at 500–650 K. (This probability limit is calculated from the ratio of this maximum number of impurity molecules in the reactor volume, $\ll 2 \times 10^{17}$, divided by the total number of collisions of H_2O molecules with the surface during the 2-min exposure.)

D. Water-Gas Shift Kinetics on Zn-Doped Cu(111)

We performed several experiments to test the influence of surface Zn on the performance of the Cu(111) surface as a WGS catalyst. We dosed Zn to the surface in a manner similar to that we have described in (*26*), except here a droplet of aqueous Zn acetate solution was dried onto the surface by heating mildly in air. The Zn overlayers thus generated gave AES and XPS spectra very similar to those described in (*26*), which indicates an oxidized zinc or ZnO species at the surface. Before reaction, the O/Zn stoichiometric ratio at the surface was high (~8, calculated as in (*26*)). Such surfaces gave no improvement or change in activity compared to clean Cu(111) for WGS at 612 K, 10 Torr H_2O, and 26 Torr CO, provided the Zn coverage was below one monolayer. After reaction, the O/Zn stoichiometry reduced to ~3 : 1, but the Zn(2*p*) XPS peak position (1021.5 eV BE with respect to the Fermi level) and the Zn(LMM) XAES position (988 eV) were still characteristic of ZnO or heavily oxidized Zn (*26*). After reaction, the Cu(2*p*) spectrum was completely metallic in character. The Zn/Cu AES and XPS ratios for these surfaces, when compared to results in (*26*), indicate Zn coverages between 0.5 and 6 monolayers, depending on the concentration of Zn acetate solution used. For the highest Zn doses, the O/Zn stoichiometry after reaction reduced to ~2 : 1. This may be due to contributions from both a ZnO_3 surface species in the first monolayer and bulk ZnO-like structure in subsequent layers. The ZnO_3 surface species is similar to that described in (*26*). The oxygen atoms in this species are undoubtedly also bonded to surface Cu atoms.

At the highest Zn coverages, there appeared to be a slight enhancement in the WGS rate (factor of ~1.6). This could be due to a simple increase in metallic Cu surface area, if the Cu emerges to cover the oxidized Zn overlayer upon heating in the reaction mixture. Such segregation behavior would be characteristic of Cu/ZnO mixtures (*26*), and could easily give a factor of 2 increase in the number of Cu surface atoms. In any case, these experiments give *no* support for a strong interaction between Cu and ZnO which leads to noteworthy improvements in Cu activity for WGS.

IV. DISCUSSION

The specific activity and kinetics of Cu(111) which we have observed here can be favorably compared with values for high-surface-area Cu/ZnO and Cu-based catalysts in the WGS reaction. This can be seen in Table 1, where we compare our site-

TABLE 1

Cu Catalysts: Specific Activities and Kinetic Parameters in Water-Gas Shift
(TOF = $A \exp(-E_a/RT)\, P_{H_2O}^n P_{CO}^m$)

Catalyst	T (K)	P_{H_2O} (Torr)	P_{CO} (Torr)	TOF[a] (site^{-1} s^{-1})	E_a (kcal mole^{-1})	Order in H_2O (= n)	Order in CO (= m)	Ref.
Cu(111)	563–683	10	26	0.02–0.4	17	0.5–1.0	0	Present
33/67 Cu/ZnO	501	304	214	0.07	16	0.7	0[b]	(3)
33/67 Cu/ZnO	563	10	26	0.02[b]				(3)
50/50 Cu/ZnO					14			(1)
23/67/10 Cu/ZnO/Al_2O_3	523	<750	<750	0.002				(5)
Cu	523	<750	<750	0.001				(5)
Cu/Al_2O_3	673	236	182	12	13.3			(6)
Cu/Al_2O_3	403					0.38	0.3	(6)

[a] Assuming 10^{15} sites cm^{-2}.
[b] Calculated from Eq. (8) in Ref. (3).

specific rates and kinetic parameters for Cu(111) with values for a variety of Cu-based catalysts in the literature. Consideration must be given to the fact that the rates and reaction orders may vary with temperature and reactant pressures. The best correlation is with the data of van Herwijnen and co-workers (*3*), who provide an analytical expression which can be used to extrapolate their data to our conditions. Their observed reaction orders and activation energy are in excellent agreement with our values, as is their extrapolated TOF. All the reported activation energies (*1, 3, 6*) fall within 3.7 kcal mole^{-1} of the value for Cu(111). The reaction orders of Grenoble *et al.* (*6*) differ from ours, but they refer to a much different regime of temperature and H_2O/CO pressure ratio. Their TOF, when corrected for differences in H_2O pressure, are in fairly good agreement with our values for Cu(111). Compared to the other entries in the table, the specific rates of Yurieva and Minyukova (*5*) seem somewhat low, although their reactant pressures, while less than 760 Torr, were not specifically reported.

Overall, it appears that the Cu(111) single-crystal surface serves as a very good kinetic model for high-surface-area, Cu-based catalysts. This would certainly be expected if the active form of Cu on high-area catalysts is metallic, since the (111) plane is the most stable surface orientation of metallic Cu (from a thermodynamic viewpoint (*27*)). Our post-reaction surface analyses also point to a very reduced catalyst under working conditions, one that is completely metallic in nature. Other workers have addressed the nature of the active Cu phase in WGS catalysts (*1, 2, 4, 5, 28, 37*), with some concluding that Cu metal is the active phase ((1) and refs. therein), and others believing that Cu ions in the metal-oxide lattice are important (*5, 28, 46*). Certainly there is no strong evidence at this stage for any synergistic relationship between Cu and ZnO in WGS catalysts except that the ZnO helps to disperse the metallic Cu phase and thereby increase its surface area. Our results supported a model where metallic Cu is the active phase for WGS. This conclusion is based upon both the agreement in Table 1 between specific activities for Cu(111) and Cu/ZnO catalysts, as well as the lack of influence of ZnO_x overlayers upon the WGS activity of Cu(111).

We will discuss our kinetics in terms of a

mechanism for the reaction which has been supported by others (*1, 3, 6–8*), involving a formate intermediate:

$$CO \rightleftharpoons CO_a \quad (1)$$

$$H_2O \rightleftharpoons H_2O_a \quad (2)$$

$$H_2O_a \xrightarrow{\text{slow}} OH_a + H_a \quad (3)$$

$$OH_a + CO_a \xrightarrow{\text{fast}} HCOO_a \quad (4)$$

$$HCOO_a \xrightarrow{\text{fast}} H_a + CO_2 \quad (5)$$

$$2H_a \xrightarrow{\text{fast}} H_2 \quad (6)$$

Surface science measurements of steps (1) and (2) on Cu surfaces yield adsorption/desorption kinetic parameters which can give us an estimate of CO and H_2O coverages under our reaction conditions. The CO/Cu(110) interaction has been analyzed in great detail (*29, 30*). In the limit of zero coverage, a sticking probability of 0.46 was observed, and desorption proceeds with a first-order desorption preexponential and activation energy of 5×10^{12} s^{-1} and 12.2 kcal $mole^{-1}$, respectively. While such exact numbers do not exist for Cu(111), qualitatively the behavior is identical for CO on Cu(111) ((*22, 31*) and refs. therein). Using the parameters from Cu(110) and assuming adsorption/desorption equilibrium, we predict a CO coverage of 8×10^{-3} at 26 Torr CO and 612 K on Cu(111). Water adsorbs molecularly on clean Cu(110) with a sticking probability of ~1 at low coverage, and desorbs molecularly in a peak at 170 K when heated at 10 K/s under UHV (*32*). Using first-order Redhead analysis (*33*), and assuming a typical desorption preexponential of 10^{13} s^{-1}, these data indicate an activation energy for desorption of 9.8 kcal $mole^{-1}$. The adsorption/desorption behavior of H_2O on Cu(111) (*34*) and Cu(110) (*32*) are also qualitatively quite similar. Again, using the Cu(110) parameters and assuming adsorption/desorption equilibrium, we predict a coverage of H_2O on Cu(111) at 612 K and 10 Torr H_2O of 5×10^{-4}. Even with an order-of-magnitude error in these predictions, it would appear that the coverages of CO and H_2O are very low under our reaction conditions. Thus, the reaction should proceed in the low-coverage limit for steps (1) and (2) above, where θ_{CO} and θ_{H_2O} are proportional to P_{CO} and P_{H_2O}, respectively.

Under these conditions, the near independence of the rate on P_{CO} and its strong increase with P_{H_2O} (Fig. 4) can be understood within the above mechanism only if step (3) proceeds slowly in hydroxyl production; but, once produced, each surface hydroxyl is rapidly consumed by CO_a to make the formate intermediate via step (4). Thus step (3) is rate controlling. It is interesting that step (4) is fast even at such low CO coverages. A similar situation occurs for the CO oxidation reaction on transition metals at high temperatures and low P_{O_2}/P_{CO} ratios. There, the CO coverage is very low but the rate, which is limited by dissociative O_2 adsorption, is independent of CO pressure (see (*43*), for example). This is related to the fact that a CO molecule has a high sticking probability (*22, 31*), and will visit a large number of sites during its lifetime on the surface (see (*44*), for example). This effect can be further understood by performing a steady-state mass balance for OH_a in our mechanism, which shows that θ_{OH} should be proportional to P_{H_2O}/θ_{CO}. However, the rate of step (4) should be proportional to the product $\theta_{OH} \times \theta_{CO}$, so that dependence upon θ_{CO} cancels out in the overall rate, in spite of its low value.

Under higher pressure and lower temperature conditions, it has been suggested that formate decomposition is rate controlling (*3*). However, equating the observed reaction rate at 612 K (TOF $\simeq$ 0.1) with the formate decomposition rate calculated using the kinetic parameters from Cu(110) (*30*), we obtain a formate coverage of only $\sim 10^{-3}$ monolayers. Unless the kinetic parameters for formate decomposition on Cu(111) and (110) are greatly different, this indicates that step (5) is very fast under our conditions and should not contribute to overall reaction kinetic parameters. Such a difference is certainly not expected since

formate decomposition kinetics is structure insensitive [36] and virtually identical on Cu(110) (*30*), Cu(100) (*35*), Cu powder (*36*), and Cu/SiO_2 (*36*). The activation energy of 13.3–17 kcal $mole^{-1}$ for WGS on various Cu surfaces (Table 1) is far below that which has been reported for the decomposition of adsorbed formate (29–31 kcal $mole^{-1}$) (*30, 36*). This further shows that step (5) above is *not* limiting the reaction rate under our conditions, and probably does not under the broader conditions of Table 1. Van Herwijnen and co-workers (*3*) would disagree with this analysis, for they found that formic acid decomposition and WGS proceed with the same rate and temperature dependence on Cu/ZnO. However, Iglesia and Bondart (*36*) and Dubois *et al.* (*42*) point out that the presence of physisorbed formic acid can cause a marked decrease in the apparent activation energy of the former, which is not occurring under WGS conditions since formic acid is not present. We should note that, at higher H_2O pressures, it is likely that processes other than H_2O dissociation will limit the reaction rate, as is generally evidenced by changes in the reaction orders with respect to H_2O and CO partial pressures (see (*3*), for example).

The TDS behavior for hydrogen desorption ($2H_a \rightarrow H_2$) on Cu(111) (*38*) proves that step (6) should also be very fast at 612 K. It is unlikely that the reverse of step (3), $H_a + OH_a \rightarrow H_2O_a$, contributes significantly under our conditions within the proposed mechanism, since the independence of rate upon P_{CO} (and CO coverage) proves that CO dominates hydroxyl consumption via step (4): $CO_a + OH_a \rightarrow HCOO_a$. If hydroxyl hydrogenation were competing seriously, the rate would increase with CO coverage.

There is some controversy in the literature concerning the probability for H_2O_a to dissociate via step (3) on Cu surfaces. On Cu(100), no dissociation was observable upon heating a monolayer of H_2O_a (*39*). Some formation of OH_a was observed by Spitzer and Luth (40) on Cu(110), although Bange *et al.* (*32*) disagree. A "few percent" of H_2O_a converts to OH_a on Cu(111) upon warming to 160 K (*34*). Oxygen adatoms aid in the conversion of H_2O_a to hydroxyls on Cu surface (*32, 34, 39*). Since O_a could be generated by beam-damage effects when studying water adsorption by surface science methods (*41*), we feel that "a few percent" of H_2O_a conversion to OH_a on Cu(111) (*34*) only sets an upper limit on the dissociation probability. The process $2(OH_a) \rightarrow H_2O + O_a$ is quite rapid even at 200 K on Cu surfaces (*32, 34*). Thus, our limit of $<10^{-6}$ for the probability for dissociative adsorption of H_2O to produce O_a on Cu(111) (Section C under results) also indicates that hydroxyl production is similarly improbable. This observation is then also consistent with step (3) above being the rate-controlling step in WGS under our conditions. The reaction probability for H_2O in WGS at 612 K is $\sim 4 \times 10^{-8}$, consistent with the above limit. We should point out that, since the rate under our conditions is controlled by step (3) in the proposed mechanism, our present results provide no new evidence concerning the latter steps in the mechanism.

An alternate surface-redox mechanism has also been suggested (*1, 4*), where OH_a, produced in step (3), further dissociates to produce oxygen adatoms (O_a), which are then consumed by CO: $CO_a + O_a \rightarrow CO_2$. This mechanism is also consistent with our observations, provided dissociative water adsorption is rate controlling. This would certainly be expected of this mechanism, since the reaction $CO_a + O_a \rightarrow CO_2$ proceeds at a high rate on Cu(111) (*22*). In this mechanism, the reverse of step (3), or hydroxyl hydrogenation, could be important.

In either mechanism, the rate is controlled by the dissociation of H_2O_a. The coverage of H_2O decreases as $\exp(E_{des}/RT)$ with increasing temperature, if we are indeed in the low-coverage limit as suggested above. (Here E_{des} is the activation energy for water desorption.) The apparent activa-

tion energy (E_a) then reflects the difference between the activation energy for this dissociation step (E_{diss}) and that for H_2O desorption (E_{des}): $E_a = E_{diss} - E_{des} = 17$ kcal mole^{-1}. Since E_{des} is near 10 kcal mole^{-1} on Cu(111) (see above), this indicates an activation energy of ~27 kcal mole^{-1} for the dissociation of an adsorbed water molecule. The reaction rate at 612 K, 10 Torr H_2O, and 26 Torr CO is 0.1 site^{-1} s^{-1}. Above, we estimated the coverage of H_2O_a under these conditions to be 5×10^{-4}. If we assume that water dissociation proceeds as a first-order process in θ_{H_2O}, this coverage and the activation energy of 27 kcal mole^{-1} allow us to calculate the preexponential factor for dissociation of an adsorbed water molecule (ν_{diss}). The result is a value of ~8×10^{11} s^{-1}, which is reasonably close to the expected value (10^{13} s^{-1}) for typical first-order processes. This lends credence to the arguments above.

We should point out that, in the alternate surface redox mechanism, if step (3) achieves a rapid equilibrium ($H_2O_a \rightleftharpoons OH_a + H_a$), then this activation energy of 27 kcal mole^{-1} should be interpreted as the sum of ΔH for this equilibrium and the activation energy for hydroxyl dissociation ($OH_a \rightarrow O_a + H_a$). The value of ν_{diss} then reflects the multiple of the H_2O coverage times the preexponential factor for hydroxyl dissociation. The reader should remember that high coverages can substantially alter surface energetics, so that extrapolation of these values to conditions of higher pressure may be uncertain.

Part of our data are not completely consistent with the above model. Note in Fig. 1 that the rate is not perfectly first-order in H_2O pressure, as there is some evidence for nonlinearity here. Our comparison to desorption kinetics indicates, however, that the H_2O coverage is extremely low at reaction temperature, in which case the water coverage and dissociation rate should be proportional to H_2O pressure. Due to the scatter in the data, we will not complicate our analysis due to this slight deviation from proportionality in the WGS rate. One possibility to explain this, however, could involve a contribution from defect sites (e.g., more active metal impurities) which bond water more strongly and dissociate it more readily. The general agreement in activity for various Cu catalysts (Table 1) would be hard to understand if such defects dominated the rate, however.

Addendum. After submission of this paper, Judd *et al.* (*45*) reported a LEED pattern for O/Cu(111) after ~10^6 Langmuir O_2 exposure at room temperature followed by annealing at 370 K. They propose a structural model for that pattern where $\theta_0 = 0.5$. Many of the features of their pattern are similar to those of our Fig. 1b, which suggests a related surface structure. Our structure was achieved with a much lower exposure, at a higher temperature.

ACKNOWLEDGMENTS

The authors acknowledge support of this work by the U.S. Department of Energy, through Morgantown Energy Technology Center. We also thank B. E. Koel for useful discussions, as well as contributions with part of the data collection. The experiments were performed at Los Alamos National Laboratory.

REFERENCES

1. Newsome, D. S., *Catal. Rev. Sci. Eng.* **21,** 275 (1980).
2. (a) Garbassi, F. and Petrini, G., *J. Catal.* **90,** 106 (1984); (b) Petrini, G., and Garbassi, F., *J. Catal.* **90,** 113 (1984).
3. (a) van Herwijnen, T., and de Jong, W. A., *J. Catal.* **63,** 83 (1980); (b) van Herwijnen, T., Guczalski, R.T., and de Jong, W. A., *J. Catal.* **63,** 94 (1980).
4. Fiolitakis, E., and Hofmann, H., *J. Catal.* **80,** 328 (1983).
5. Yurieva, T. M., and Minyukova, T. P., *React. Kinet. Catal. Lett. (USSR)* **29,** 55 (1985).
6. Grenoble, D. C., Estadt, M. M., and Ollis, D. F., *J. Catal.* **67,** 90 (1981).
7. Klier, K., Young, C. W., and Nunan, J. G., *Ind. Eng. Chem. Fundam.* **25,** 36 (1986).
8. Bybell, D. C., Deutsch, P. P., Herman, R. G., Himelfarb, P. B., Nunan, J. G., Young, C. W., Bogdan, C. E., Simmons, G. W., and Klier, K., *Prepr. Petrol. Div. Amer. Chem. Soc.* **31,** 282 (1986).
9. Kantschewa, M., Delannay, F., Jeziorowski, H., Delgado, E., Eder, S., Ertl, G., and Knozinger, H., *J. Catal.* **87,** 482 (1984).
10. Hou, P., Meeker, D., and Wise, H., *J. Catal.* **80,** 280 (1983).

11. Rethwisch, D. G., Phillips, J., Chen, Y., Hayden, T. F., and Dumesic, J. A., *J. Catal.* **91,** 167 (1985).
12. Campbell, C. T., and Koel, B. E., *Surface Sci.*, in press.
13. Campbell, C. T., and Koel, B. E., in preparation.
14. Campbell, C. T., and Paffett, M. T., *Surf. Sci.* **139,** 396 (1984).
15. Russell, J. N., Gates, S. M., and Yates, J. T., *Surf. Sci.* **163,** 516 (1985).
16. Ertl, G., *Surf. Sci.* **6,** 208 (1967).
17. Simmons, G. W., Mitchell, D. F., and Lawless, K. R., *Surf. Sci.* **8,** 130 (1967).
18. Hollins, P., and Pritchard, J., *Surf. Sci.* **134,** 91 (1983).
19. Spitzer, A., and Luth, H., *Surf. Sci.* **118,** 136 (1982).
20. Niehus, H., *Surf. Sci.* **130,** 41 (1983).
21. Thurgate, S. M., and Jennings, P. J., *Surf. Sci.* **131,** 309 (1983).
22. Habraken, F., Kieffer, E. P., and Bootsma, G. A., *Surf. Sci.* **83,** 45 (1979).
23. Dubois, L. H., *Surf. Sci.* **119,** 399 (1982).
24. Davis, L. E., *et al.*, "Handbook of Auger Electron Spectroscopy," Perkin–Elmer Corp., Eden Prairie, MN 1983.
25. Strohmeier, B. R., Leyden, D. E., Field, R. S., and Hercules, D. M., *J. Catal.* **94,** 514 (1985).
26. Campbell, C. T., Daube, K. A., and White, J. M., *Surface Sci.*, in press.
27. Anderson, J. R., "Structure of Metallic Catalysts." Academic, New York, 1975.
28. Yurieva, T. M., Boreskov, G. K., and Gruver, V. S., *Kinet. Katal.* **10,** 294 (1969).
29. Harendt, G., Goschnick, J., and Hirschwald, W., *Surf. Sci.* **152**(3), 453 (1985).
30. Wachs, I. E., and Madix, R. J., *J. Catal.* **53,** 208 (1978).
31. (a) Hayden, B. E., Kretzschmar, K., and Bradshaw, A. M., *Surf. Sci.* **155,** 553 (1985); (b) Tracy, J. C., *J. Chem. Phys.* **56,** 2748 (1972).
32. Bange, K., Grider, D. E., Madey, T. E., and Sass, J. K., *Surf. Sci.* **136,** 38 (1984).
33. Redhead, P. A., *Vacuum* **12,** 203 (1962).
34. Au, C. T., Breza, J., and Roberts, M. W., *Chem. Phys. Lett.* **66,** 340 (1979).
35. Sexton, B. A., *Surf. Sci.* **88,** 319 (1979).
36. Iglesia, E., and Boudart, M., *J. Catal.* **81,** 214 (1983).
37. Vlaic, G., Bart, J., Cavigiolo, W., Pianzola, B., and Mobilio, S., *J. Catal.* **96,** 314 (1985).
38. Greuter, F., and Plummer, E. W., *Solid State Commun.* **48,** 37 (1983).
39. Spitzer, A., Ritz, A., and Luth, H., *Surf. Sci.* **152**(3) 543 (1985).
40. Spitzer, A., and Luth, H., *Surf. Sci.* **120,** 376 (1982); *Surf. Sci.* **160,** 353 (1985).
41. Sass, J. K., and Richardson, N. V., *Surf. Sci.* **139** L204 (1984).
42. Dubois, L. H., Ellis, T. H., Zegarski, B. R., and Kevan, S. D., *Surf. Sci.* **172,** 385 (1986).
43. Campbell, C. T., and White, J. M., *J. Catal.* **54,** 289 (1978).
44. Campbell, C. T., Ertl, G., Kuipers, H., and Segner, J., *Surf. Sci.* **107,** 207 (1981).
45. Judd, R. W., Hollins, P., and Pritchard, J., *Surf. Sci.* **171,** 643 (1986).
46. Okamoto, Y., Konishi, Y., Fukino, K., Imanaka, T., and Teranishi, S., Int. Congr. Catal., [Proc.], 8th, 1984, 5, V159–V170 (Verlag Chemie, Weinheim, FRG).